

## Longitudinal tear detection method of conveyor belt based on audio-visual fusion

Che, Jian; Qiao, Tiezhu; Yang, Yi; Zhang, Haitao; Pang, Yusong

**DOI**

[10.1016/j.measurement.2021.109152](https://doi.org/10.1016/j.measurement.2021.109152)

**Publication date**

2021

**Document Version**

Accepted author manuscript

**Published in**

Measurement: Journal of the International Measurement Confederation

**Citation (APA)**

Che, J., Qiao, T., Yang, Y., Zhang, H., & Pang, Y. (2021). Longitudinal tear detection method of conveyor belt based on audio-visual fusion. *Measurement: Journal of the International Measurement Confederation*, 176, Article 109152. <https://doi.org/10.1016/j.measurement.2021.109152>

**Important note**

To cite this publication, please use the final published version (if applicable).  
Please check the document version above.

**Copyright**

Other than for strictly personal use, it is not permitted to download, forward or distribute the text or part of it, without the consent of the author(s) and/or copyright holder(s), unless the work is under an open content license such as Creative Commons.

**Takedown policy**

Please contact us and provide details if you believe this document breaches copyrights.  
We will remove access to the work immediately and investigate your claim.

# Longitudinal Tear Detection Method of Conveyor Belt Based on Audio-visual Fusion

Jian Che<sup>a,b</sup>, Tiezhu Qiao<sup>a,b,\*</sup>, Yi Yang<sup>a,b</sup>, Haitao Zhang<sup>a,b</sup>, Yusong Pang<sup>c</sup>,

<sup>a</sup> Key Laboratory of Advanced Transducers and Intelligent Control System, Ministry of Education, Taiyuan University of Technology, Taiyuan 030024, China

<sup>b</sup> College of Physics and Optoelectronics, Taiyuan University of Technology, Taiyuan 030024, China

<sup>c</sup> Section of Transport Engineering and Logistic, Faculty of Mechanical, Maritime and Materials Engineering, Delft University of Technology, 2628 CD Delft, Netherlands

**Abstract:** Conveyor belt tear detection is a very important part of coal mine safety production. In this paper, a new method of detecting conveyor belt damage named audio-visual fusion (AVF) detection method is proposed. The AVF method uses both a visible light CCD and a microphone array to collect images and sounds of the conveyor belt in different running states. By processing and analyzing the collected images and sounds, the image and sound features of normal, tear and scratch can be extracted respectively. Then the extracted features of images and sounds are fused and classified by machine learning algorithm. The results show that the accuracy of AVF method for conveyor belt scratch is 93.66%, and the accuracy of longitudinal tear is higher than 96.23%. Compared with existing methods AVF method overcomes the limitation of visual detection condition, and is more accurate and reliable for conveyor belt tear detection.

**Keywords:** Audio-visual feature extraction; Feature fusion; Longitudinal tear detection method; Machine learning

## 1. Introduction

Belt conveyor is an indispensable transportation equipment in coal mine production. Conveyor belt is the most accident-prone part of the whole belt conveyor [1],[2]. During the operation of the conveyor belt, gangue, anchored bolt and other metal hard objects at the transfer point may scratch and tear the conveyor belt[3],[4]. Learn from the research methods of turning tool wear[5],[6] we discover conveyor belt scratches are a precursor to longitudinal tear and longitudinal tear is longer and more common than horizontal tearing of conveyor belts[7]. Owing to the long transport distance of coal, if a longitudinal tearing accident occurs, the entire belt may be replaced, and normal production and transportation of the coal mine cannot be restored for a long period of time, which causes huge economic losses. If workers do not find the accident in time, it will lead to blockage of coal mine roadway, and would even cause casualties. Therefore, fast and accurate damage detection methods for conveyor belts are essential

---

\* Corresponding author  
E-mail address: [qiaotiezhu@tyut.edu.cn](mailto:qiaotiezhu@tyut.edu.cn) (Tiezhu Qiao).

35 for coal mine safety production.

36 At present, it has become a trend to use computer vision technology to detect  
37 conveyor belt longitudinal tear. For example, Qiao and Li[8] used a laser and a surface  
38 light source to build a visual recognition system for longitudinal tear of the conveyor  
39 belt. Yang et al. [9]proposed a fast image segmentation algorithm based on line array  
40 CCD camera. Wang et al. [10] proposed a non-contact conveyor belt tear detection  
41 method based on image processing and pattern recognition. Wang and Sun[11] proposes  
42 a conveyor belt longitudinal tear detection method based on Haar-AdaBoost and  
43 Cascade algorithm under uneven light. However, the visible light CCD (Charge Coupled  
44 Device) may be affected by the environment in the mine due to the dark, watery and  
45 dusty working environment in the mine. Therefore, the detection accuracy will be  
46 greatly affected. Qiao et al. [12] proposed an binocular vision detection method based  
47 on the fusion of infrared and visible light. Yang and Qiao[13] proposed a longitudinal  
48 tear warning method based on infrared image ROI selection and image binarization.  
49 Yang and Qiao[14] proposed Infrared spectrum analysis method for detection and early  
50 warning of longitudinal tear. The infrared method is used to detect tearing, the principle  
51 is that when the conveyor belt is damaged by friction with hard impurities, thermal  
52 radiation is generated through the conveyor belt and detected by infrared CCD,  
53 However, if the tear process of the conveyor belt is slow and the temperature cannot  
54 rise rapidly, the thermal radiation cannot be detected by infrared CCD through the  
55 conveyor belt in time and there will be missed detection. Therefore, the validity and  
56 accuracy of test results will be affected as before. In order to adapt to the complex  
57 environment under the coal mine and improve the accuracy of tear detection, a new  
58 detection method which enables to adapt to the dark and dusty environment as well as  
59 to meet timely and accurate demand is needed.

60 At present, computer vision and sound detection technology are developing rapidly,  
61 the two are widely used in medical[15],[16], transportation[17],[18], security  
62 inspection[19],[20] and other fields such as emotion recognition[21] and acoustic scene  
63 classification[22]. Computer vision technology can replace the human eye for  
64 recognition, tracking and measurement, but the quality of computer vision image is very  
65 sensitive to obstacles, occlusion and light conditions. On the one hand, audio detection  
66 is equivalent to human ears. The sound signal is not affected by the light can still  
67 transmit information effectively when encountering obstacles. Sound signal has the  
68 advantages of convenient collection, low cost and space saving. The use of sound  
69 detection can be very good auxiliary computer vision and applied to the detection  
70 system. Audio-visual detection is not only non-contact but also more accurate and  
71 stable. When the conveyor belt rubs against hard impurities, it will produce a sharp  
72 sound, which can be well distinguished from the normal operation of the conveyor belt.

73 Image and sound are the most obvious features of longitudinal tearing or scratching of  
74 the conveyor belt. In summary, this paper proposes a longitudinal tear detection method  
75 based on audio-visual fusion (AVF) conveyor belt. The AVF method can not only adapt  
76 to the complex environment under the coal mine, but also detect the scratches of the  
77 conveyor belt more accurately.

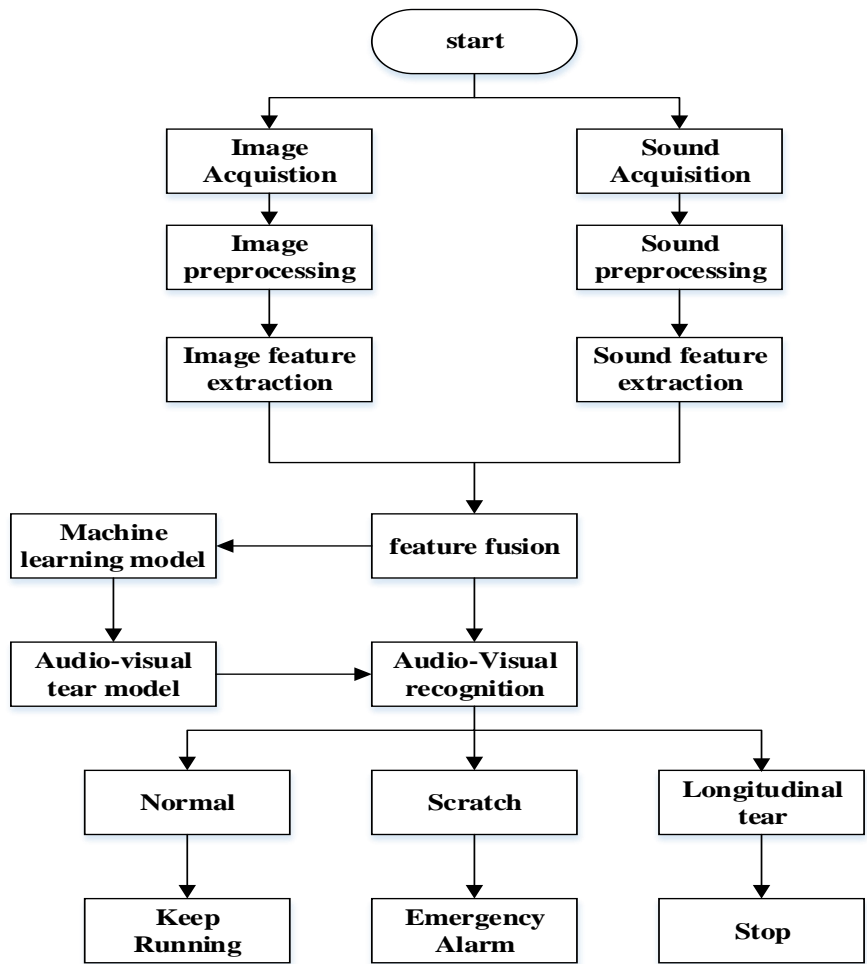
78 Sound image information fusion and feature extraction are two key steps in AVF  
79 method. In terms of information fusion, according to the theory of information  
80 fusion[23], Data fusion can be done on the feature layer, data layer and decision layer.  
81 Since the image and sound are heterogeneous in nature, and their data have no  
82 correlation with each other, it is almost impossible to carry out information fusion on  
83 the data layer. When the conveyor belt is torn longitudinally, there is a certain  
84 correlation between the generation of tear and the sound produced. If they are fused at  
85 the decision layer, their correlation will be separated, which will lead to the decrease of  
86 detection accuracy. Therefore, the feature layer is selected for the data fusion of sound  
87 and image.

88 In terms of feature extraction, we extracted MFCC(Mel-Frequency Cepstral  
89 Coefficients), Spectral centroid, Short-time energy, ZCR(Zero Crossing Rate) and  
90 Spectral roll-off as sound features[24]. For image features, we mainly want to obtain  
91 the image contour information when the conveyor belt is torn longitudinally, so we  
92 extract the HOG (Histogram of Oriented Gradient) feature. After extracting the features  
93 of sound and image, network fuses two features. The fused features were sent to the  
94 machine learning model for training, and the trained model was used to identify the  
95 new tear. Compared with the previous methods. The AVF method adds sound features  
96 to the traditional computer vision detection of longitudinal tear of the conveyor belt. It  
97 not only overcomes the difficulty of collecting data with visible light CCD in the  
98 complex environment of coal mines, but also effectively solves the problem of missed  
99 detection by infrared detection methods. We analyzed the image and sound features,  
100 and for the first time proposed the fusion of sound features and image features in the  
101 feature layer, which eliminate the redundancy and contradiction between image and  
102 sound information and complement each other, and improve the real-time and reliability  
103 of the longitudinal tear detection of the conveyor belt.

104 The organization of this paper is as follows. Section 2 mainly introduces AVF  
105 methods, which includes sound feature extraction, image feature extraction, image and  
106 sound feature fusion and machine learning model. Section 3 gives the experimental  
107 results and analysis to verify the AVF method, we compared the accuracy of using  
108 image features alone and using audio-visual fusion features, and compared the AVF  
109 method with some visual detection methods that have been proposed, followed by the  
110 conclusions and possible improvements are discussed in Section 4.

111 **2. AVF method**

112 This section mainly introduces the method of AVF, which consists of four parts  
113 including image feature extraction, sound feature extraction, feature fusion and  
114 machine learning methods. Firstly, the image of tear and is scratch captured by visible  
115 light CCD and its features are extracted. Secondly, we use a microphone array to collect  
116 tear and scratch sounds and extract sound features. Thirdly, the fusion of image features  
117 and sound features at the feature layer, the fused audio-visual features were sent to the  
118 machine learning model for training. Finally, the existing tear or scratch can be  
119 distinguished by audio-visual fusion detection model of conveyor belt longitudinal  
120 tearing. The AVF method flowchart is shown in Fig.1. Each section is described as  
121 following section.



122  
123 **Fig.1.Flow chart of AVF method**

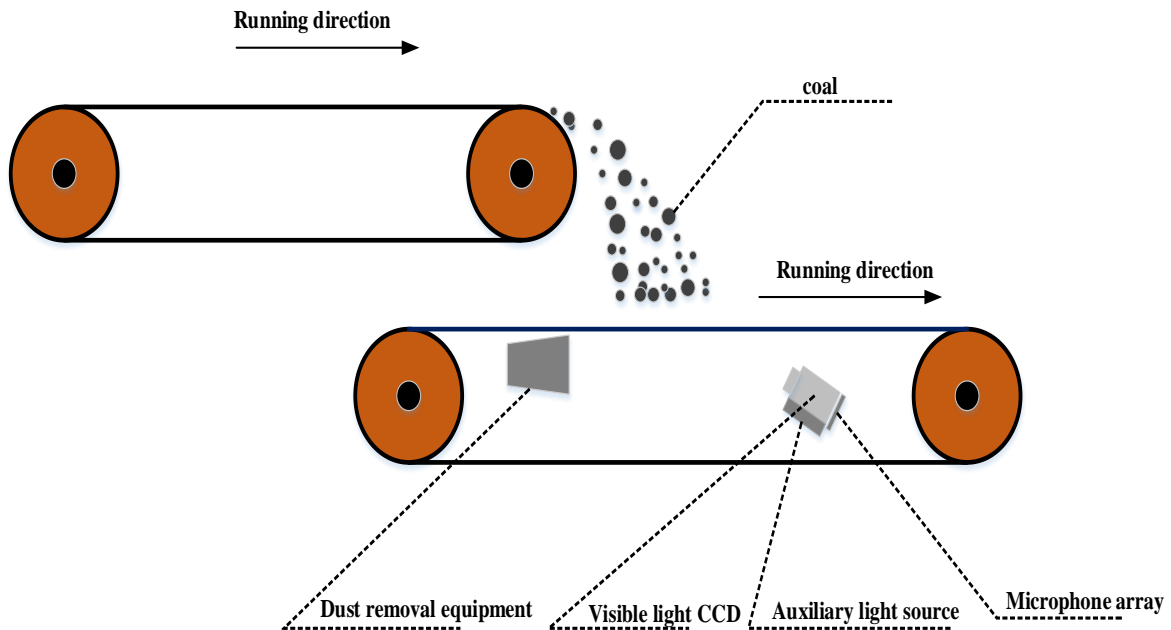
124 **2.1. Data acquisition**

125 In order to train a good conveyor belt longitudinal tear audio-visual detection model,

126 it is very important to collect audio-visual data. We use visible light CCD and  
127 microphone to collect the image and sound data of normal operation, scratch and  
128 longitudinal tear of the conveyor belt at the same time. The specific acquisition methods  
129 of image and sound are as follows

### 130 2.1.1. Image acquisition

131 Since most of the longitudinal tear occurs at the transfer point of the conveyor  
132 belt[25] , we install the visible light CCD under the belt near the transfer point. Due to  
133 the dark and dusty working environment in the mine, it is hard to capture clear tear  
134 images using a visible light CCD alone, which greatly affects the accuracy of  
135 longitudinal tear detection. In order to overcome the impact of the complex  
136 environment of the coal mine on the captured images, auxiliary light sources and dust  
137 removal equipment need to be installed. We install the dust removal equipment on the  
138 front of the visible light CCD, and install the auxiliary light source below the visible  
139 light CCD as shown in Fig.2. The visible light CCD collects images of the under  
140 different conditions. The collected images are divided into three categories: the normal  
141 images, the scratched image and the longitudinal tear image are shown in Fig.3.



142

143

**Fig. 2.** Dust removal equipment of visible light CCD and auxiliary light source



(a) (b) (c)  
**Fig. 3.** The collected images:(a) normal image. (b) tear image (c) scratch image

### 2.1.2 Sound acquisition

Microphone array is installed at the bottom of visible light CCD to collect the sound of the conveyor belt during normal transportation, the sound of scratches and the sound of tear. Setting the sampling frequency to 44.1kHz. In order to eliminate the influence of aliasing, high-order harmonic distortion, and other factors on the quality of the sound signal caused by sound collection equipment and environmental sound, we need to preprocess the collected original sound. Pre-processing the sound signal under different conditions of the conveyor belt includes two parts: pre-emphasis and framing and windowing, pre-emphasis compensates for the high-frequency part of the sound, which improves the signal-to-noise ratio of the high-frequency part of the sound signal. Windowing divides the continuous sound signal into independent frame signals and smooth the frame signals, which is convenient for calculation in the frequency domain.

### 2.2 Data preprocessing and feature extraction

We preprocess the collected images and extract image features from the preprocessed images. For tear and scratch images, we found through experiments that the contour features of tears and scratches have good performance, so the contour features of the edges of tears and scratches are extracted. By comparing the sound of longitudinal tear, the sound of scratch and the sound of normal operation of the conveyor belt, it is found that there are obvious differences among them. Therefore, sound features can be used as an important feature in longitudinal tear detection of conveyor belt. There are two parts included in sound feature extraction: sound pretreatment and feature extraction. In this paper, MFCC, ZCR, Spectral-centroid, Short-term energy and Spectral roll-off are extracted as the feature of sound.

170 2.2.1 Image preprocessing

171 In the collected visible light image, the damage area is obvious. However, in the  
172 background, except for the damaged area, in the actual working environment of coal  
173 mine, there will be some scratches and stains in the pictures we take. In order to better  
174 extract the damage features, we use median filtering to filter the image [26]. Assuming  
175 that the conveyor belt image captured by the Visible light CCD is  $g(s, t)$  then the image  
176 processing formula with the pixel value  $f(x, y)$  after the median filtering is as follows:

177 
$$f(x, y) = \underset{(s,t)=S_{xy}}{\text{median}}\{g(s, t)\} \quad (1)$$

178 In order to extract features in the next step, grayscale the image after median filtering.  
179 As shown in Fig.4.

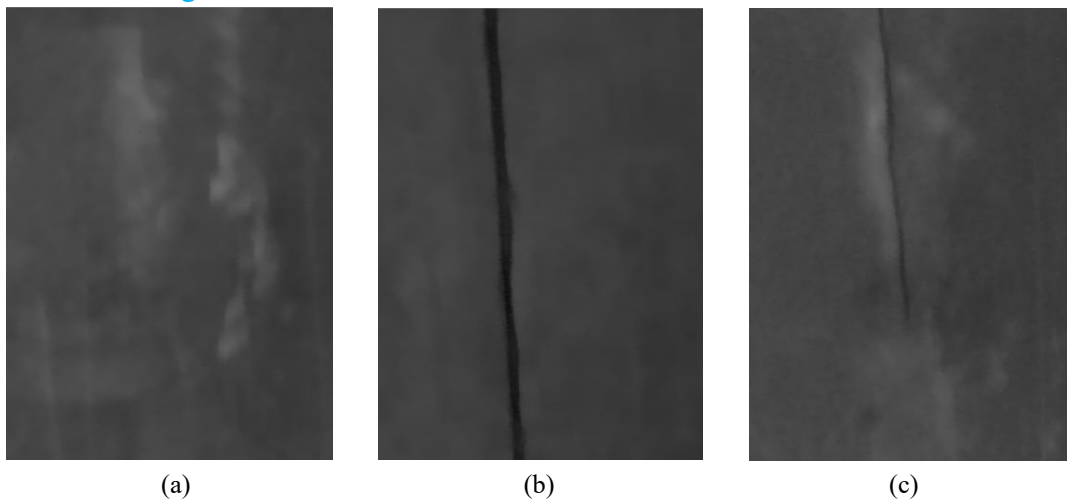


Fig. 4. The processed images:(a) normal image; (b) tear image; (c) scratch image.

184 2.2.2. Image HOG feature extraction

185 Dalal and Triggs[27] proposed an image feature description algorithm HOG based  
186 on gradient direction. HOG algorithm calculates and statistics the gradient and direction  
187 of image pixels, and calculates gradient histogram of local images to construct features,  
188 which can describe the edge of the detection object well. Compared with other image  
189 feature extraction algorithms, HOG operates on the local grid cells of the image, so it  
190 can maintain good invariance to image geometric and optical deformations, and can  
191 tolerate different forms between tears feature. The steps for the HOG algorithm are  
192 described as follows.

193 (1) Gamma correction

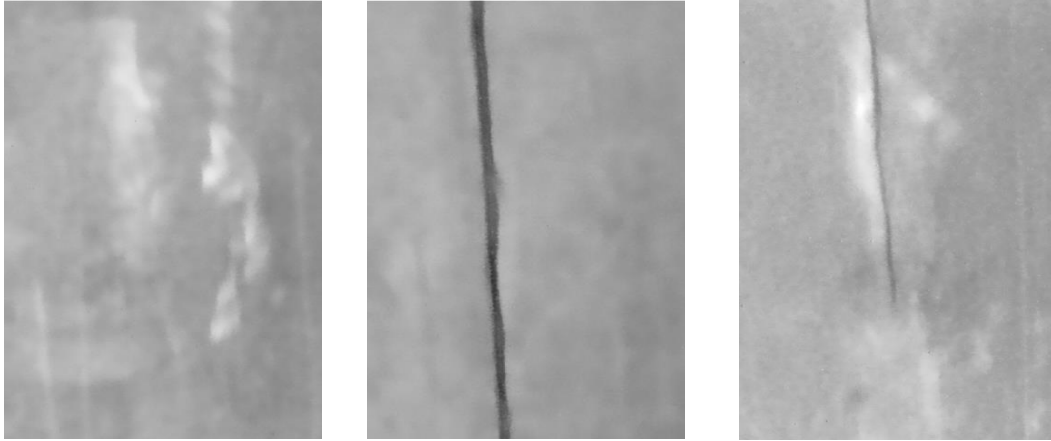
194 In order to overcome the impact of the dark and dusty mine on local shadows and  
195 image brightness changes, highlight the damaged parts of the picture, we first used  
196 gamma correction to process the image. Gamma correction can improve the image  
197 contrast effect of the darker or brighter part of the image. The formula of Gamma  
198 correction is as follows:



199

$$f(x) = x^\gamma \quad (2)$$

200 Where  $x$  is the pixel value of the image, and  $\gamma$  is the Gamma correction coefficient.  
 201 Here,  $f(x)$  is the output pixel value. In this paper, the correction coefficient is 0.8, and  
 202 the image after gamma correction is shown in [Fig. 5](#)



(a)

(b)

(c)

**Fig. 5.** The Image after gamma correction:(a) normal image; (b) tear image; (c) scratch image.

(2) Calculate image gradient

We use the statistical gradient method to obtain the longitudinal tearing profile information of the conveyor, the gradient in mathematics is actually the first derivative. The gradient of a continuous image at a certain pixel point can be calculated by the following formula.

$$G_x(x, y) = H(x+1, y) - H(x-1, y) \quad (3)$$

$$G_y(x, y) = H(x, y+1) - H(x, y-1) \quad (4)$$

Where  $G_x(x, y)$  is the vertical gradient at point  $(x, y)$ ,  $G_y(x, y)$  is the horizontal gradient,  $H(x, y)$  is the pixel value at point  $(x, y)$ , the gradient amplitude  $G(x, y)$  and direction  $a(x, y)$  at point  $(x, y)$  are calculated as follows:

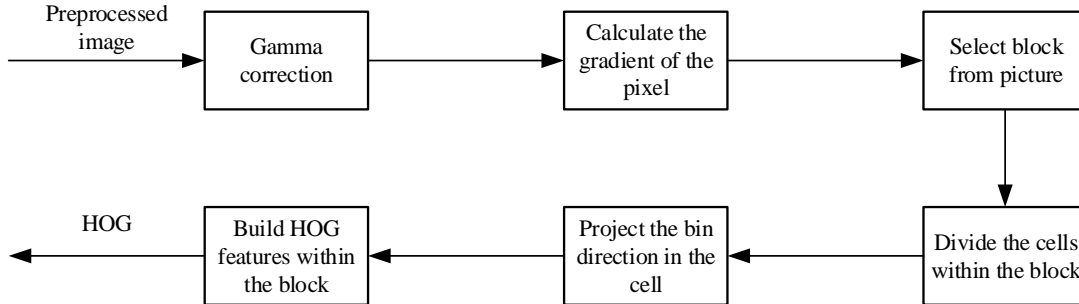
$$G(x, y) = \sqrt{G_x(x, y)^2 + G_y(x, y)^2} \quad (5)$$

$$a(x, y) = \tan^{-1}\left(\frac{G_y(x, y)}{G_x(x, y)}\right) \quad (6)$$

(3) Calculate HOG feature

First, the image was divided into  $8 * 8$  pixels of small cell, then the gradient direction of 360 degrees of cell can be divided into 9 bins, 9 bins of the histogram is used to statistics the  $8 * 8$  pixels gradient information, finally to calculate the pixel gradient direction projection to its corresponding histogram, In this way, the weighted projection of the gradient size and direction of each pixel in the cell on the histogram is the corresponding 9-dimensional feature vector of the cell. We use four cells to form a block of  $16 * 16$  pixels. It's going to join up to form a  $36 * 1$  member vector. Then, the

226 block window moves with a fixed step size (8 pixels per step) to normalized the  
 227 histogram, thus generating a standardized 36\*1 vector for each move. The 36 features  
 228 obtained after each movement are concatenated together as the final feature of our  
 229 image. The HOG feature extraction flowchart is shown in the Fig. 6



230

231

**Fig. 6.** HOG feature extraction flowchart

### 232 2.2.3. Sound preprocessing

#### 233 (1) Pre-emphasis

234 Because of the conveyor belt longitudinal tear sound signal collection belt is often  
 235 affected by various noises under the mine, the high-frequency acoustic signal will  
 236 attenuate. Therefore, before the sound signal processing, We should enhance the high  
 237 frequency part of the sound to effectively reduce the output noise, obtain more  
 238 frequency-domain information, so as to facilitate sound feature extraction[28]. Pre-  
 239 emphasis usually expression of the transfer function is:

240

$$H(Z) = 1 - aZ^{-1} \quad (7)$$

241 Where  $a$  is the pre-emphasis coefficient, which is 0.97 in this experiment (usually  
 242 selected between 0.9 and 1)

#### 243 (2) Framing and Windowing

244 Because of the sound signal remains unchanged and relatively stable in a short time  
 245 range, it is possible to divide sound signal into some short segments for processing Each  
 246 short segment is called a frame. We use overlapping segmentation method to divide  
 247 frames. The overlapping segmentation method enhances the correlation between frames  
 248 and facilitates the smooth transition between them, the overlapping part is called frame  
 249 shift. In this paper, frame length  $N=1024$  and frame shift  $T=256$ , the sampling  
 250 frequency is set to 44.1KHZ, so each frame is 23.2ms. In order to obtain a smoother  
 251 spectrum, we use hamming window for framing. The hamming window calculation  
 252 formula is:

253

$$w(n) = \begin{cases} (1-a) - a \cos[2\pi n / (N-1)], & 0 \leq n \leq N \\ 0, & \text{others} \end{cases} \quad (8)$$

254 Where  $N$  is the frame length, and different  $a$  will generate different hamming  
 255 windows and here we choose  $a=0.46$ , after determining the window function, add a  
 256 window to the pre-emphasis sound signal, the formulas for framing and windowing are  
 257 as follows:

$$258 \quad s'(n) = s(n) * w(n), \quad (9)$$

259 Where,  $s(n)$  is the original sound of the  $n$ -the frame,  $s'(n)$  is the sound signal of  
 260 the  $n$ -the frame after windowing and framing processing.

#### 261 2.2.4. Sound Feature extraction

##### 262 (1) MFCC

263 MFCC has been widely used in audio signal analysis[29]. Although MFCC is mainly  
 264 designed for voice processing, but we found that it can be used to analyze the damage  
 265 of conveyor belt. The frequency perceived by the human auditory system of low-  
 266 frequency sounds and the physical frequency of the sound are approximately linear; the  
 267 frequency perceived by high-frequency sounds and the physical frequency of the sound  
 268 are approximately logarithmic. The relationship between the Mel frequency and the  
 269 physical frequency the relationship is shown in the formula.

$$270 \quad f_{mel} = 2595 \log_{10} \left( 1 + \frac{f_{hz}}{700} \right) \quad (10)$$

271 Where  $f$  is the frequency the specific steps to extract MFCC parameters from sound  
 272 signals in different damage states is as follows:

273 ● After the preprocessing of sound signal, we convert the audio signal in the time-  
 274 frequency domain, its main implementation is Discrete Fourier Transform (DFT). The  
 275 DFT input is a sequence of frames windowed to signal  $s'(n)$ , the output is the  
 276 complex number  $x_n(k)$  containing  $N$  frequency bands. The definition of DFT is as  
 277 follows:

$$278 \quad x_n(k) = \sum_{n=0}^{N-1} s'(n) e^{-j2\pi kn/N}, \quad 0 \leq k \leq N \quad (11)$$

279 Where  $k$  is the  $k$ th spectrum of the Fourier transform, and  $N$  is the number of points  
 280 of the Fourier transform.

281 ● Through the Mel filter. The Mel filter is composed of a triangular bandpass filter,  
 282 which can convert the frequency spectrum into Smooth processing to remove the  
 283 influence of harmonics and highlight the formants of the original sound, the  
 284 frequency response of the triangle filter  $H_m(K)$  is:

285

$$H_m(k) \begin{cases} 0, & k < f(m-1) \\ \frac{2(k-f(m-1))}{(f(m+1)-f(m-1))(f(m)-f(m-1))}, & f(m-1) \leq k < f(m) \\ \frac{2(f(m+1)-k)}{(f(m+1)-f(m-1))(f(m+1)-f(m))}, & f(m) \leq k \leq f(m+1) \\ 0, & k > f(m+1) \end{cases} \quad (12)$$

287 Where  $H_m(k)$  satisfies:

$$288 \quad \sum_{m=0}^{M-1} H_m(k) = 1 \quad (13)$$

289 ● Take the logarithmic energy, and perform logarithmic operation on the signal  
290 passing through the triangular filter bank. The logarithmic energy output by the  $m$ -  
291 th Mel filter is shown in the following formula.

$$292 \quad S(m) = \ln\left(\sum_{k=0}^{N-1} |x_n(k)|^2 H_m(k)\right) \quad 0 < m < M \quad (14)$$

293 Where  $M$  is the number of Mel scale triangle filters, we select 26 in this paper.

294 ● Through the discrete cosine transform of the energy logarithm  $S(m)$  to MFCC.

$$295 \quad C(m) = \sum_{l=0}^{M-1} S(m) \cos\left(\frac{\pi l(i-0.5)}{M}\right), \quad l = 0, 1, 2, \dots, L \quad (15)$$

296 Perform discrete cosine transform on  $S(m)$  to obtain the Mel-scale cepstral  
297 parameter  $C(m)$ ,  $L$  is the order of the MFCC coefficient, usually set to 12-16. In  
298 this paper,  $L = 13$ .

299 (2) Short-Time Energy

300 As the energy of the sound signal changes with time, the sound energy of tear,  
301 scratches and normal operation of the conveyor belt are significantly different.  
302 Therefore, the analysis of short-time energy can describe the characteristic changes in  
303 different states of the conveyor belt. The short-time energy is calculated as follows:

$$304 \quad E_n = \sum_{m=0}^{N-1} s_n^2(m) \quad (16)$$

305 Where  $s_n(m)$  is the  $n$ th frame sound signal,  $m$  is for window position.

306 (3) ZCR

307 The zero-crossing rate represents the rate at which the symbols of the sound signal  
308 change, the ZCR is mainly used for the recognition when the background noise is large.  
309 The calculation formula is as follows:

$$310 \quad ZCR_n = \frac{1}{2} \sum_{m=0}^{N-1} [\text{sgn}(s_n(m)) - \text{sgn}(s_n(m+1))] \quad (17)$$

311 Where  $\text{sgn}()$  is the sign function, the formula is as follows:

$$\text{sgn}(x) = \begin{cases} 1, & x \geq 0 \\ -1, & x < 0 \end{cases} \quad (18)$$

#### 313 (4) Spectral centroid

314 Spectral centroid is one of the important parameters to describe the timbre attributes.  
 315 It is the frequency averaged by energy weighted within a certain frequency range, the  
 316 spectral centroid describes the brightness of sound. It is the important information of  
 317 the frequency distribution and energy distribution of the sound signal. The calculation  
 318 formula is:

$$SC_n = \frac{\sum_{f=0}^{F_s/2} f S_n(f)}{\sum_{f=0}^{F_s/2} S_n(f)} \quad (19)$$

320 Where  $f$  is the sound signal frequency,  $S_n(f)$  is the spectral energy formula of the  
 321 corresponding frequency after the discrete Fourier transform of the continuous time  
 322 domain signal  $s_n(m)$  as follows:

$$S_n(f) = \sum_{m=0}^{N-1} s_n(m) e^{-j2\pi km/N} \quad (20)$$

325 Where  $N$  is the frame length.

#### 326 (5) Spectral roll-off

327 Spectrum roll-off is the change of the spectrum amplitude when the frequency is  
 328 lower than a certain set value. According to the characteristics of the spectrum roll-off,  
 329 the slope of the spectrum shape can be measured. The calculation formula of spectrum  
 330 roll-off is as follows:

$$\sum_{k=0}^m |S_n(k)| = \theta \sum_{k=0}^{N-1} |S_n(k)| \quad (21)$$

332 Where  $\theta$  is the threshold, and its value range is 0.85~0.99, In this paper it is 0.85

### 333 2.3. Feature fusion

334 In the feature layer, we fused the sound features and image features of the conveyor  
 335 belt under different operating states, including data normalization processing and PCA  
 336 dimensionality reduction.

#### 337 2.3.1. Data normalization

338 We serialized the acquired image features and sound features to obtain the new audio-  
 339 visual fusion eigen matrix  $X$ , and then carried out data normalization processing on the  
 340 acquired new audio-visual fusion eigen matrix. The calculation formula is

$$x_j^{(i)} = \frac{a_j^{(i)} - \mu_j}{s_j} \quad (22)$$

342 Where  $a_j^{(i)}$  is the  $j$  eigenvalue of  $i$  samples,  $\mu_j$  represents the mean value of the  $j$   
343 feature, and  $s_j$  represents the range of the  $j$  feature, that is:  $s_j = \max(a_j^{(i)}) -$   
344  $\min(a_j^{(i)})$ .

### 345 2.3.2.PCA

346 PCA is a dimensionality reduction algorithm, which can convert high-dimensional  
347 data into low-dimensional data with minimal loss[30]. We use PCA algorithm to  
348 process audio-visual fusion features, extract useful information and remove redundant  
349 information. After the normalization of the data, the audio-visual fusion feature matrix  
350  $X$  was obtained, and the covariance matrix was first calculated:

$$351 \quad C = \frac{1}{m} X^T X \quad (23)$$

352 Where  $C$  is the covariance matrix, and then the singular value decomposition is  
353 used to calculate the eigenvectors of the covariance matrix.

$$354 \quad [U, S, V] = svd(C) \quad (24)$$

355 After the characteristic matrix is obtained, dimensionality reduction can be carried  
356 out on the data. Assuming that the value before dimensionality reduction is  $x^{(i)}$ , the  
357 formula of  $Z^{(i)}$  dimension reduction is as follows:

$$358 \quad Z^{(i)} = U_{reduce}^T x^{(i)} \quad (25)$$

359 Where  $U_{reduce} = [u^{(1)}, u^{(2)}, \dots, u^{(k)}]$  is principal component characteristic matrix.

### 360 2.4. Machine learning model

361 We classify the collected audiovisual data of conveyor belt damage. In this paper, we  
362 have selected three machine learning algorithms, K-nearest neighbors(KNN) algorithm  
363 is simple to implement, suitable for multi-classification problems, and not sensitive to  
364 abnormal points[31], support vector machine (SVM) biggest characteristic is the  
365 maximum distance can be structured decision boundary, generalization error rate is low,  
366 It has high robustness, due to the small sample of audio-visual data we collect, SVM is  
367 better than other algorithm in the case of fewer data sets[32]. The Random Forest (RF)  
368 algorithm is a classification algorithm that combines multiple weak classifiers (decision  
369 trees) into a strong classifier. The fusion of the output of multiple classifiers not only  
370 helps to improve the accuracy of classification, but also factors such as outliers and  
371 noise in the data are well tolerated and are not prone to overfitting[33].

### 372 **3.Experiment and analysis**

373 In this section, we are simulating the actual environment of coal mines and show the  
374 experimental results of the AVF method on the audio-visual data set we collected.

#### 375 3.1. Experiment setup

376 In order to prove the effectiveness of the AVF method, we built an experimental  
377 platform and since the laboratory itself is located in the basement, we turn off the  
378 laboratory light, use only auxiliary light source, and blow dust around visible CCD and  
379 conveyor belt to simulate the underground environment of the mine to collect audio-  
380 visual data, the picture of the conveyor belt, visible light CCD and microphone array is  
381 shown in Fig.7. Using steel wire conveyor belt, the specific parameters of the conveyor  
382 belt are as follows: length 13 meters, width 1 meter, thickness 15 mm, longitudinal  
383 tensile strength 1250 N/mm, the speed is 4m/s. We installed anchor bolt between the  
384 upper and lower conveyor belts to simulate the tear of the upper belt. The visible light  
385 CCD is an area-array industrial camera with a resolution of 1280\*1080 and a frame rate  
386 of 60 fps, the sound acquisition device is a four-array microphone, in the AVF method  
387 experiment, we simulate the tear and scratch of the conveyor belt to collect the images  
388 and sounds under different running states of the conveyor belt, we set the sampling  
389 frequency of the sound to 44.1KHz and the duration of each segment to 1.2s, all sounds  
390 are in wav format. A computer is used for sound and image processing and machine  
391 learning modeling. The specific parameters of the computer is: CPU is Inter Core i7-  
392 7700 3.6GHz, memory is 16GB. The experiment simulated the dark and dusty working  
393 environment of the coal mine.

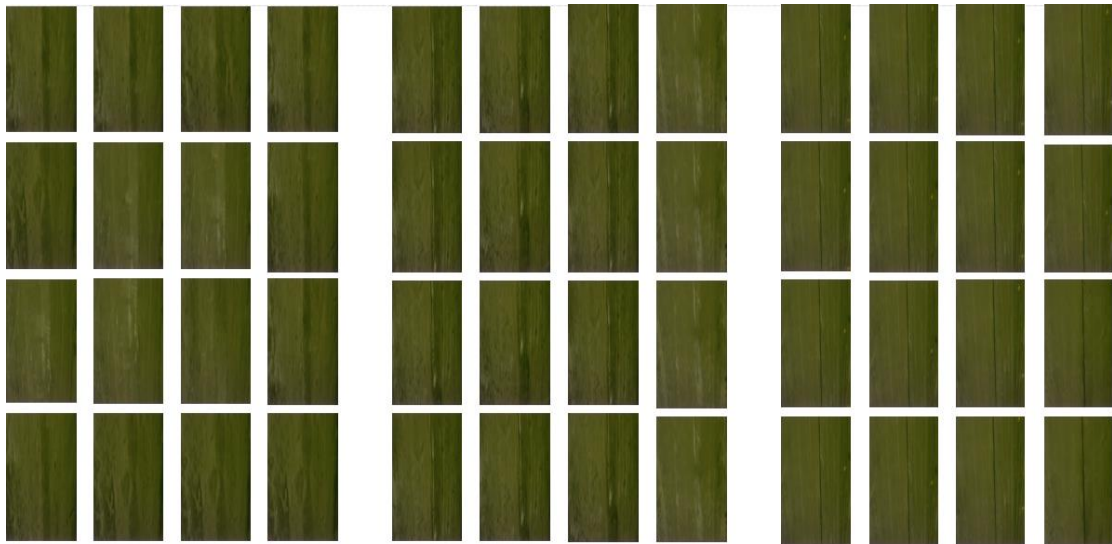
394 We first place the metal anchor bolt on the surface of the conveyor belt, turn on the  
395 conveyor belt to allow it to run normally, then adjust the depth of the anchor bolt so that  
396 it slightly penetrates the conveyor belt to simulate the conveyor belt scratch, and then  
397 adjust the depth of the anchor bolt to penetrate the conveyor belt to make it through  
398 conveyor belt simulates the belt tear. According to the different depth of bolt insertion,  
399 the normal operation of the conveyor belt, the belt scratch and longitudinal tear of the  
400 conveyor belt are respectively presented, a total of 2,600 including 1000 pictures  
401 normal, 800 pictures of the tear and 800 pictures of the scratch were taken as the image  
402 data set, the image data set is shown in Fig.8. At the same time, added the collected  
403 noise of the conveyor belt running in the mine to the collected sound fragments to  
404 simulate the working environment of the coal mine. We collected a total of 2600 sound  
405 segments corresponding to the pictures of the conveyor belt in different states as our  
406 sound data set including 1000 sound segments during normal operation, 800 sound  
407 segments during longitudinal tearing and 800 sound segments during scratch. The  
408 schematic diagram of the AVF method experiment is shown in Fig.9.



(a)

(b)

**Fig. 7.** The experiment platform:(a) Conveyor belt, (b) Visible light CCD and microphone array



(a)

(b)

(c)

**Fig. 8.** The experimental samples:(a) The normal sample, (b)The scratch sample, (c)The Tear sample

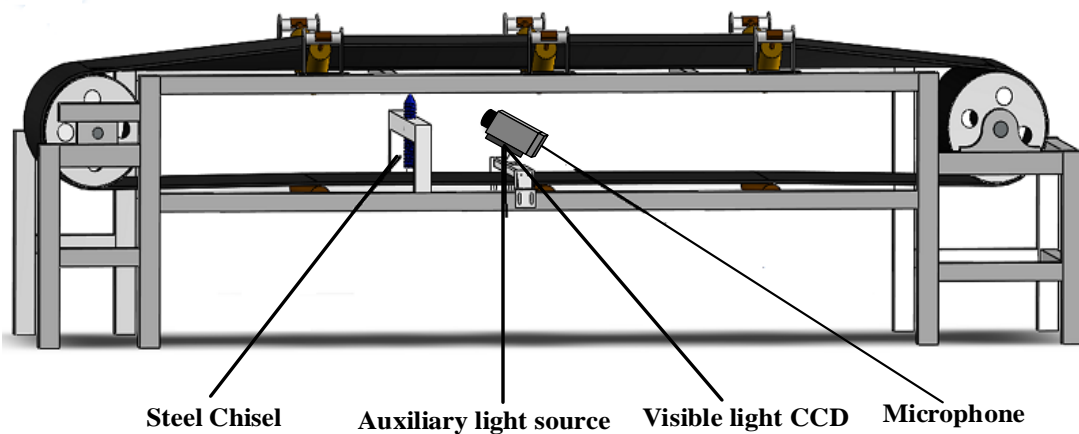


**Fig. 9.** Schematic diagram of AVF method experiment



417 All experiments are performing by python3.7, and development platform is Pycharm.  
 418 The experimental data is divided into three parts, including conveyor belt normal  
 419 operation of audio-visual data, conveyor belt longitudinal tear of audio-visual data and  
 420 conveyor belt scratches of audio-visual data, then the three parts of audio-visual data  
 421 respectively do image and sound of feature extraction and feature fusion to get the audio-  
 422 visual fusion features of different running states of the conveyor belt. The audio-visual  
 423 fusion features of different conveyor belt operation states were input into the classifier  
 424 we selected. The main parameters of the three classifiers are shown in Table.1. We  
 425 choose these parameters through experiments to optimize the classification performance  
 426 of conveyor belt audio-visual fusion data as much as possible, and perform 3-fold cross-  
 427 validation to get the final audio-visual fusion detection model. The experimental results  
 428 and analysis are as followed section:

429 **Table 1**

430 The main parameters of each machine learning model

Models	Main parameters of the model		
<b>KNN</b>	K: 1, 5, 10, 15, 20, 25	Distance: 'euclidean', 'cityblock', 'minkowski'	
<b>SVM</b>	Kernel function: rbf	C: $10^{-1}$	Gamma: $2^{-12}$ , $2^{-10}$ , $2^{-8}$ , $2^{-4}$ , $2^{-2}$ , $2^0$ , $2^2$
<b>RF</b>	n_estimators : $2^3$ , $2^4$ , $2^5$ , $2^6$	min_sample_leaf: 0, 5, 10, 20	max_features: 5

### 431 3.2. Experiment result and analysis

432 We performed PCA analysis on the audio-visual features and visual features, and the  
 433 results are given in Fig.10, from Fig.10 We can see that the overall score of the audio-  
 434 visual features is higher than that of the visual features alone, the audio-visual feature  
 435 dimension has the highest score at 850. We compared three different machine learning  
 436 classifiers. The results of the KNN-based AVF method are given in Table 2, from Table  
 437 2 we can see the average accuracy is 93.9%, the average detection time of 27.6ms. The  
 438 results of the SVM-based AVF method are given in Table 3, from Table 3 we can see  
 439 the average accuracy is 96.23%, the average detection time of 25.7ms. The results of  
 440 the RF-based AVF method are given in Table 4, from Table 4 we can see the average  
 441 accuracy is 95.63%, the average detection time of 29.99ms. The overall result is shown  
 442 in Fig.11, from Fig.11, we can see the accuracy rate of the AVF method based on SVM  
 443 is 2.23% higher than that based on KNN. The detection speed is 1.9ms faster, and the  
 444 accuracy of detection is 0.6% higher than that based on RF. The detection speed is  
 445 4.92ms faster, SVM has advantages in detection accuracy and detection time compared  
 446 with RF and KNN.

447 Comparing the image detection method with the AVF method are given in Table 5,  
 448 from Table 5 we can see the overall detection accuracy of AVF method is 96.23%, while

449 that of image detection method is 92.25%. Therefore, the method of AVF is better than  
 450 the method of image detection. As shown in the Fig.12, AVF method for all kinds of  
 451 conveyor belt with damage detection accuracy higher than that of image detection  
 452 especially for conveyor belt scratch detection, AVF detection method average accuracy  
 453 is 93.66%, and the image detection method used alone is 87.16%. This shows that AVF  
 454 detection method has higher accuracy in scratch detection, Due to the precursor of the  
 455 longitudinal tear of the conveyor belt when the conveyor belt is scratched, it is very  
 456 important for the safety production of the coal mine to detect the conveyor belt scratches,  
 457 the timely detection of the conveyor belt scratches can reduce the occurrence of  
 458 longitudinal tearing of the conveyor belt.

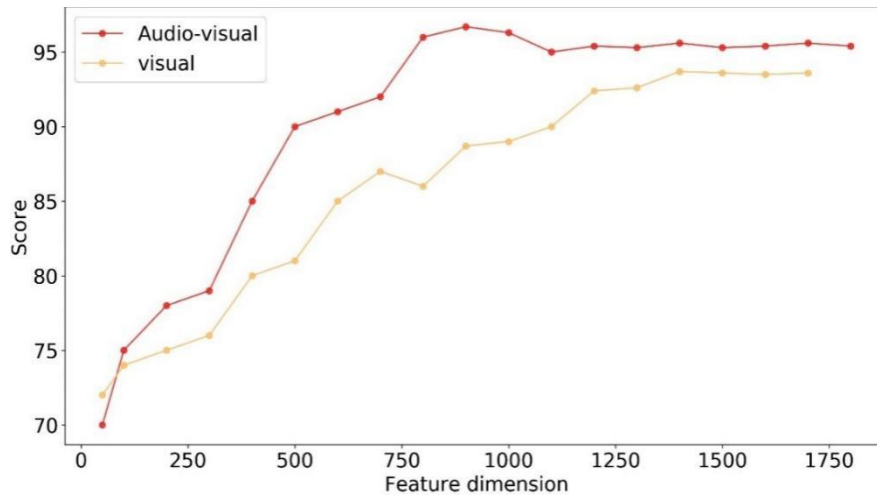
459 In order to better evaluate our method, and Compare with Qiao's IBVD method and  
 460 Gong Xian Wang' method We calculated the accuracy, recall rate and FPR (false positive  
 461 rate) of the tear sample and normal sample.

$$462 \quad recall = \frac{TP}{TP + FN} \times 100\% \quad (26)$$

$$463 \quad FPR = \frac{FP}{FP + TN} \times 100\% \quad (27)$$

$$464 \quad accuracy = \frac{TP + TN}{TP + TN + FP + FN} \times 100\% \quad (28)$$

465 Where TP is the number of tear samples detected as tears, FN is the number of normal  
 466 samples detected as tears, FP is the number of tear samples detected as normal, and TN  
 467 is the number of normal samples detected as normal, the results are shown in Table 6,  
 468 compared with the IBVD method, the AVF method has better accuracy, recall, and FPR.  
 469 Compared with the Gong Xianwang'method, both have high detection accuracy, but the  
 470 Gong Xianwang'method processing time is 96.5ms The AVF method processing time is  
 471 25.7ms, so the AVF method is more in line with the needs of real-time detection of coal  
 472 mines.



473

474

**Fig.10.** Score by applying PCA

**Table 2**

Detection results of AVF based on KNN

Experiment	Tear sample			Scratch sample			Normal sample			Accuray	Average detection time (ms)
	tear	scratch	normal	tear	scratch	normal	tear	scratch	normal		
1	190	8	2	17	182	1	1	9	190	93.6%	27.89
2	188	10	2	15	179	6	2	5	193	93.3%	26.90
3	193	5	2	10	184	6	1	7	192	94.8%	28.24

**Table 3**

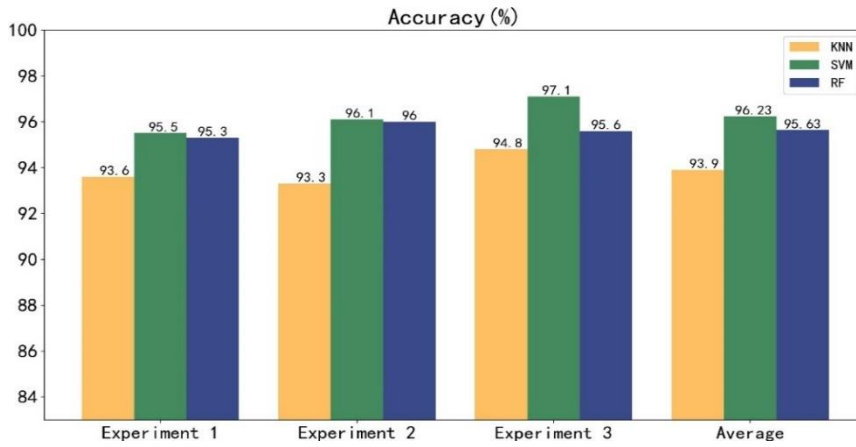
Detection results of AVF based on SVM

Experiment	Tear sample			Scratch sample			Normal sample			Accuray	Average detection time (ms)
	tear	scratch	normal	tear	scratch	normal	tear	scratch	normal		
1	191	8	1	13	185	2	1	2	197	95.5%	24.89
2	192	6	2	10	187	3	0	2	198	96.1%	25.79
3	193	6	1	9	190	1	0	0	200	97.1%	26.44

**Table 4**

Detection results of AVF based on RF

Experiment	Tear sample			Scratch sample			Normal sample			Accuray	Average detection time (ms)
	tear	scratch	normal	tear	scratch	normal	tear	scratch	normal		
1	192	7	1	13	184	3	2	2	196	95.3%	30.88
2	190	5	5	11	188	1	0	2	198	96.0%	29.47
3	192	6	2	10	187	3	0	5	195	95.6%	29.64



475

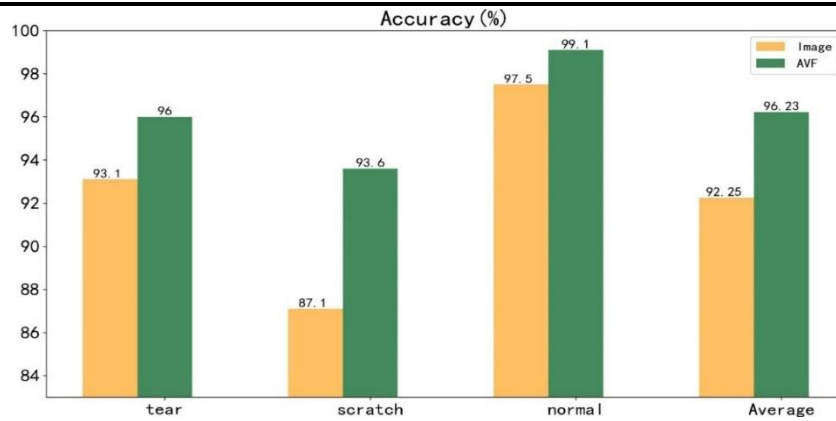
476

**Fig.11.** Accuracy comparison of three machine learning models.

**Table 5**

The image detection results based on SVM

Experiment	Tear sample			Scratch sample			Normal sample			Accuracy	Average detection time (ms)
	tear	scratch	normal	tear	scratch	normal	tear	scratch	normal		
1	187	12	1	15	179	6	2	4	194	93.3%	22.88
2	188	10	2	20	174	6	0	5	195	92.8%	23.47
3	184	10	6	25	170	5	0	4	196	91.6%	24.64



477

478

**Fig. 12.** Accuracy comparison between the AVF method and the image method

479

**Table 6**

480

Comparison of AVF method, IBVD method and Gong ian Wang method

Methods	recall	accuracy	FPR	Processing time (ms)
AVF	98.96%	96.23%	3.8%	25.7
Gong XianWang'method	93%	95.5%	5%	96.5
IBVD	90.16%	86.75%	12.07%	26.7

## 481 **4. Conclusions**

482 In this paper, we investigated a conveyor belt tear detection method based on sound  
483 and visual features, in order to adapt to the complex environment in coal mines and  
484 improve the detection accuracy. Visible light CCD is used to collect images of different  
485 running states of the conveyor belt, while the microphone array is used to collect sounds  
486 corresponding to different images. By processing and analyzing the collected images  
487 and sounds, we extracted normal, tear and scratch image features and sound features  
488 respectively. Then the extracted image and sound features fused and the machine  
489 learning algorithm is used for training and classification. The experimental findings the  
490 overall accuracy of AVF method is above 96.23%, and the recall rate is 98.96%, and  
491 FPR is 3.8% and the detection accuracy of scratches on conveyor belt is 93.6%. In terms  
492 of longitudinal tear detection Compared with the IBVD method and Gong Xian  
493 wang'method, the AVF method has better accuracy, recall and FPR. The average  
494 detection time of the AVF method is 25.7ms. In the next step of research, we can use  
495 deep learning to automatically extract the features of sound and images, and further  
496 improve the detection accuracy and generalization of the AVF method and we can also  
497 use better experimental platforms and equipment to improve the real-time performance  
498 of our algorithms. To sum up, AVF method can not only adapt to the complex  
499 environment under coal mine, but also to better achieve early warning of longitudinal  
500 tear.

## 501 **Acknowledgements**

502 This work is supported by the National Natural Science Foundation of China-Shanxi  
503 coal-based low-carbon joint fund (Grant No. U1810121) ; Funds for Local Scientific  
504 and Technological Development under the Guidance of the Central Government(Grant  
505 No.YDZX20201400001796)

## 506 **References**

- 507 [1] D. He, Y. Pang, G. Lodewijks, Green operations of belt conveyors by means of speed control, *Applied*  
508 *Energy*, 188 (2017) 330-341.
- 509 [2] M. Andrejiova, A. Grincova, D. Marasova, ANALYSIS OF TENSILE PROPERTIES OF WORN FABRIC  
510 CONVEYOR BELTS WITH RENOVATED COVER AND WITH THE DIFFERENT CARCASS TYPE, *Eksplatacja I*  
511 *Niezawodnosc-Maintenance and Reliability*, 22 (2020) 472-481.
- 512 [3] G. Fedorko, V. Molnar, D. Marasova, A. Grincova, M. Dovica, J. Zivcak, T. Toth, N. Husakova, Failure  
513 analysis of belt conveyor damage caused by the falling material. Part I: Experimental measurements and  
514 regression models, *Engineering Failure Analysis*, 36 (2014) 30-38.
- 515 [4] T. Qiao, Y. Duan, B. Jin, Infrared spectra imaging mechanism and modelling of the transport of hazard  
516 belt, *Materials Research Innovations*, 19 (2015) 92-97.
- 517 [5] M. Kuntoglu, H. Saglam, Investigation of progressive tool wear for determining of optimized  
518 machining parameters in turning, *Measurement*, 140 (2019) 427-436.

519 [6] A. Aslan, Optimization and analysis of process parameters for flank wear, cutting forces and vibration  
520 in turning of AISI 5140: A comprehensive study, *Measurement*, 163 (2020).

521 [7] M. Barburiski, Analysis of the mechanical properties of conveyor belts on the three main stages of  
522 production, *Journal of Industrial Textiles*, 45 (2016) 1322-1334.

523 [8] T. Qiao, X. Li, Y. Pang, Y. Lu, F. Wang, B. Jin, Research on conditional characteristics vision real-time  
524 detection system for conveyor belt longitudinal tear, *Let Science Measurement & Technology*, 11 (2017)  
525 955-960.

526 [9] Y. Yang, C. Miao, X. Li, X. Mei, On-line conveyor belts inspection based on machine vision, *Optik*, 125  
527 (2014) 5803-5807.

528 [10] C. Wang, J. Zhang, The research on the monitoring system for conveyor belt based on pattern  
529 recognition, in: J.H. Wu, M. Zhao, B. Wu (Eds.) *Intelligent System and Applied Material*, Pts 1 and 22012,  
530 pp. 622-625.

531 [11] G. Wang, L. Zhang, H. Sun, C. Zhu, Longitudinal tear detection of conveyor belt under uneven light  
532 based on Haar-AdaBoost and Cascade algorithm, *Measurement*, 168 (2021).

533 [12] T. Qiao, L. Chen, Y. Pang, G. Yan, C. Miao, Integrative binocular vision detection method based on  
534 infrared and visible light fusion for conveyor belts longitudinal tear, *Measurement*, 110 (2017) 192-201.

535 [13] Y. Yang, C. Hou, T. Qiao, H. Zhang, L. Ma, Longitudinal tear early-warning method for conveyor belt  
536 based on infrared vision, *Measurement*, 147 (2019).

537 [14] R. Yang, T. Qiao, Y. Pang, Y. Yang, H. Zhang, G. Yan, Infrared spectrum analysis method for detection  
538 and early warning of longitudinal tear of mine conveyor belt, *Measurement*, 165 (2020).

539 [15] A. Qayyum, S.M. Anwar, M. Awais, M. Majid, Medical image retrieval using deep convolutional  
540 neural network, *Neurocomputing*, 266 (2017) 8-20.

541 [16] D. Kumar, P. Carvalho, M. Antunes, R.P. Paiva, J. Henriques, Noise detection during heart sound  
542 recording using periodicity signatures, *Physiological Measurement*, 32 (2011) 599-618.

543 [17] Y. Kato, T. Hayashi, T. Kitagawa, Detection of extraneous abnormal sounds affecting road traffic noise  
544 by use of a necessary condition method, *Applied Acoustics*, 67 (2006) 1009-1021.

545 [18] X. Hu, X. Ye, D. Zhang, L. Wu, Vehicle Detection Technology Based on Cascading Classifiers of Multi-  
546 Feature Integration, *International Journal of Pattern Recognition and Artificial Intelligence*, 31 (2017).

547 [19] M. Guerrieri, G. Parla, C. Celauro, Digital image analysis technique for measuring railway track  
548 defects and ballast gradation, *Measurement*, 113 (2018) 137-147.

549 [20] H. Kim, E. Ahn, S. Cho, M. Shin, S.-H. Sim, Comparative analysis of image binarization methods for  
550 crack identification in concrete structures, *Cement and Concrete Research*, 99 (2017) 53-61.

551 [21] S. Zhang, S. Zhang, T. Huang, W. Gao, Q. Tian, Learning Affective Features With a Hybrid Deep Model  
552 for Audio-Visual Emotion Recognition, *IEEE Transactions on Circuits and Systems for Video Technology*,  
553 28 (2018) 3030-3043.

554 [22] L. Yang, L. Tao, X. Chen, X. Gu, Multi-scale semantic feature fusion and data augmentation for  
555 acoustic scene classification, *Applied Acoustics*, 163 (2020).

556 [23] Y. Li, D.K. Jha, A. Ray, T.A. Wettergren, Information Fusion of Passive Sensors for Detection of Moving  
557 Targets in Dynamic Environments, *Ieee Transactions on Cybernetics*, 47 (2017) 93-104.

558 [24] A.J. Eronen, V.T. Peltonen, J.T. Tuomi, A.P. Klapuri, S. Fagerlund, T. Sorsa, G. Lorho, J. Huopaniemi,  
559 Audio-based context recognition, *Ieee Transactions on Audio Speech and Language Processing*, 14 (2006)  
560 321-329.

561 [25] A. Grincova, M. Andrejiova, D. Marasova, S. Khouri, Measurement and determination of the  
562 absorbed impact energy for conveyor belts of various structures under impact loading, *Measurement*,

563 131 (2019) 362-371.

564 [26] M. Storath, A. Weinmann, Fast Median Filtering for Phase or Orientation Data, *Ieee Transactions*  
565 *on Pattern Analysis and Machine Intelligence*, 40 (2018) 639-652.

566 [27] N. Dalal, B. Triggs, Histograms of oriented gradients for human detection, in: C. Schmid, S. Soatto,  
567 C. Tomasi (Eds.) 2005 *Ieee Computer Society Conference on Computer Vision and Pattern Recognition*,  
568 Vol 1, *Proceedings2005*, pp. 886-893.

569 [28] X. Zhou, J. Wang, H. Hu, W. Dai, L. Wei, H. Mao, *Ieee*, Recognition of Infant's Emotions and Needs  
570 from Speech Signals, 2016 *Ieee International Conference on Systems, Man, and Cybernetics2016*, pp.  
571 4620-4625.

572 [29] A. Maurya, D. Kumar, R.K. Agarwal, Speaker Recognition for Hindi Speech Signal using MFCC-GMM  
573 Approach, in: J. Mathew, A.K. Singh (Eds.) 6th *International Conference on Smart Computing and*  
574 *Communications2018*, pp. 880-887.

575 [30] X. Zeng, Q. Wang, C. Zhang, H. Cai, *Ieee*, Feature Selection Based on ReliefF and PCA for Underwater  
576 Sound Classification, 2013.

577 [31] K. Hwang, S.-Y. Lee, Environmental Audio Scene and Activity Recognition through Mobile-based  
578 Crowdsourcing, *Ieee Transactions on Consumer Electronics*, 58 (2012) 700-705.

579 [32] C.-W. Hsu, C.-J. Lin, A comparison of methods for multiclass support vector machines, *IEEE*  
580 *transactions on neural networks*, 13 (2002) 415-425.

581 [33] V. Svetnik, A. Liaw, C. Tong, J.C. Culberson, R.P. Sheridan, B.P. Feuston, Random forest: a  
582 classification and regression tool for compound classification and QSAR modeling, *Journal of chemical*  
583 *information and computer sciences*, 43 (2003) 1947-1958.

584